

Probing the rest-frame of the Universe with near-IR cosmic infrared background

A. Kashlinsky¹ * and F. Atrio-Barandela² †

¹ Code 665, Observational Cosmology Lab, NASA Goddard Space Flight Center, Greenbelt, MD 20771 and SSAI, Lanham, MD 20706

² Department of Fundamental Physics, University of Salamanca, 37008 Salamanca, Spain

Accepted 22 April 2022. Received 13 April 2022; in original form 16 March 2022

ABSTRACT

While the cosmic microwave background (CMB) dipole is largely assumed entirely kinematic, there appears evidence that a part of it is primordial. Such possibility arises in models implying a tilt, interpreted as a dark flow, across the observable Universe. The kinematic nature of the entire CMB dipole can be probed using the dipole of cosmic backgrounds from galaxies after the last scattering. The near-IR cosmic infrared background (CIB) spectral energy distribution leads to an amplified dipole compared to the CMB. The CIB dipole is affected by galaxy clustering, decreasing with fainter, more distant galaxies, and by Solar System emissions and Galactic dust, which dominate the net CIB cosmological dipole in the optical/near-IR. We propose a technique that enables an accurate measurement of the kinematic near-IR CIB dipole. The CIB, effectively the integrated galaxy light (IGL), would be reconstructed from resolved galaxies in the forthcoming space-borne wide surveys covering four bands 0.9 to 2.5 μm . The galaxies will be sub-selected from the identified magnitude range where the dipole component from galaxy clustering is below the expected kinematic dipole. Using this technique the dipole can be measured in each of the bands at the statistical signal-to-noise $S/N \gtrsim 50\text{--}100$ with the forthcoming *Euclid* and *Roman* surveys, isolating CMB dipole's kinematic nature.

Key words: (cosmology:) early Universe - (cosmology:) diffuse radiation - cosmology: observations - cosmology: miscellaneous

The cosmic microwave background (CMB) dipole is $\delta T_{\text{CMB,dip}} = 3.346\text{mK}$ toward $(l, b)_{\text{Gal}} = (263.85, 48.25)^\circ$ measured with signal-to-noise ratio $(S/N) \gtrsim 200$ (Kogut et al. 1993; Fixsen et al. 1994). Its amplitude $D_{\text{CMB}} \equiv \delta T_{\text{CMB,dip}}/T_{\text{CMB}} = 1.25 \times 10^{-3}$ is mostly, but not unanimously (Gunn 1988), interpreted as Sun's motion at $V_{\text{CMB}} = 370$ km/sec if CMB traces the Universe's rest-frame commonly identified as the universal expansion's rest-frame.

There appeared assertions contradicting CMB dipole's kinematic interpretation. Analysis of the cumulative kinematic Sunyaev-Zeldovich dipole at CMB locations from an all-sky X-ray cluster sample suggested what was termed the dark flow of the clusters with respect to CMB extending to $\sim 1\text{Gpc}$, the signal persisting in WMAP 3,5,7,9 yr CMB data (Kashlinsky et al. 2008, 2009, 2010, 2012a) and Planck 1-yr data (Atrio-Barandela 2013; Atrio-Barandela et al. 2015). Comparing gravity dipole with velocity provides similar tests (Villumsen & Strauss 1987) and a non-kinematic CMB dipole would be broadly consistent with the misalignment in direction and/or amplitude of the gravitational force reconstructed from galaxy and cluster catalogs from the CMB dipole (e.g. Gunn 1988; Lavaux et al. 2010; Erdođdu et al. 2006; Kocevski & Ebeling 2006; Wiltshire et al. 2013), the various claims of peculiar flows and their properties (e.g. Mathewson et al. 1992; Lauer & Postman 1992; Ma et al. 2011; Colin et al. 2019), the radio-counts dipole (Nodland & Ralston 1997; Jain & Ralston 1999; Singal 2011), the recent *WISE* source-counts dipole (Secrest et al. 2021) and

the anisotropy in X-ray cluster scaling relations (Migkas et al. 2020). Such measurements achieved only a limited significance, $S/N \sim (3\text{--}4)$, necessitating new ideas for reaching higher S/N required to robustly probe the CMB dipole's kinematic nature.

Before inflation was developed, it was proposed that CMB dipole may be primordial, not entirely kinematic (King & Ellis 1973; Matzner 1980). Cosmological (inflation-produced) curvature perturbations have zero intrinsic dipole at last scattering (Turner 1991), so primordial CMB dipole would reflect pre-inflationary conditions from tilt (King & Ellis 1973) by space inhomogeneities before inflation (Turner 1991) pushed beyond the cosmological horizon as constrained by the CMB quadrupole anisotropy (Kashlinsky et al. 1994; Turner 1991; Grishchuk 1992; Das et al. 2021; Tiwari et al. 2022), or could arise from entanglement of our Universe with super-horizon domains in certain Multiverse models (Mersini-Houghton & Holman 2009).

The CMB dipole nature can be probed with dipoles of cosmic backgrounds (CBs) from galaxies after the last scattering, which reflect the universal expansion rest-frame. If the Sun moves at $V \ll c$ relative to distant sources producing the CB its intensity I_ν , at frequency ν would have dipole in Sun's rest-frame known as the Compton-Getting effect for cosmic rays (e.g. Gleeson & Axford 1968):

$$d_\nu = (3 - \alpha_{\nu,\infty}) \frac{V}{c} \bar{I}_\nu \quad (1)$$

where $\alpha_{\nu,\infty} = \partial \ln I_\nu / \partial \ln \nu$ and the subscript ∞ indicates I_ν from integrating over the entire range of fluxes/magnitudes of the sources contributing to the given band. Eq. 1 follows since the Lorentz transformation leaves I_ν/ν^3 invariant (Peebles & Wilkinson 1968).

* E-mail: Alexander.Kashlinsky@nasa.gov

† E-mail: atrio@usal.es

If CMB traces the Universe’s rest-frame, $V = V_{\text{CMB}}$ for any CB. Various wavelength CBs exhibit $\alpha_{\nu, \infty} < 2$ such that their dipole amplitude gets *amplified* compared to the CMB dipole, if purely kinematic: such wavelengths include X-rays (Fabian & Warwick 1979), radio (Ellis & Baldwin 1984; Itoh et al. 2010), and sub-mm (Kashlinsky 2005; Fixsen & Kashlinsky 2011). An all-sky CB dipole measured with signal/noise S/N will have its direction probed with the directional accuracy of $\Delta\Theta_{\text{dipole}} \simeq \sqrt{2}(S/N)^{-1}$ radian (Fixsen & Kashlinsky 2011).

The near-IR CIB has the well-defined $\alpha_{\nu, \infty} \ll 2$ from $< 1\mu\text{m}$ to $\simeq 4\mu\text{m}$ and, with enough sky, its (amplified) dipole can be probed to resolve deviations from the CMB dipole in amplitude and direction, provided contributions from diffuse Galactic (cirrus) and Solar System (zodi) foregrounds, and from galaxy clustering are negligible. In this *Letter* we demonstrate that the foreground contributions dominate the cosmological dipole for the *net* near-IR CIB and propose a method to eliminate them with the integrated galaxy light (IGL) part of the CIB by using resolved galaxies. This technique is applicable to any sufficiently wide-field sky survey in which individual galaxies can be identified and which goes deep enough to minimize the dipole due to large-scale structure. Such configurations may be available with the cosmic infrared background (CIB) from the forthcoming space missions *Roman* (Spergel et al. 2015) and *Euclid* (Laureijs et al. 2011), which has an ongoing near-IR CIB program (LIBRAE 2013; Kashlinsky et al. 2018). We then identify the CIB configuration for a highly precise measurement of the CIB dipole in these surveys to resolve the kinematic nature of the long-known CMB dipole and discuss the various other components of the proposed measurement and how the near-IR CIB dipole is spectrally distinguished from any remaining foreground contribution.

1 NET NEAR-IR CIB DIPOLE VS FOREGROUNDS

The net CIB is made up of unresolved CIB and the part due to resolved galaxies. Fig. 1a shows I_{ν} integrated over known galaxies from counts data; its contribution peaks at $m_{\text{AB}} \sim 20$ (Fig. 1 in Kashlinsky et al. 2019, and below). Red line shows the fit using observed galaxy spectra (Windhorst et al. 2011; Driver et al. 2016). Yellow-filled regions show the empirical CIB reconstruction from the multi-epoch, multi-wavelength known galaxy luminosity function data (Helgason et al. 2012, hereafter HRK). Black lines show the HRK-reconstructed background (“default”, the optimal value); the yellow shaded region marks the high-faint-end (HFE) and low-faint-end (LFE) limits of the observed luminosity function data used by HRK. The contribution from new sources implied by the source-subtracted CIB fluctuations uncovered in *Spitzer* measurements (Kashlinsky et al. 2005, 2007b, 2012b) contributes little to the overall mean CIB (Kashlinsky et al. 2007a) and will not enter the final configuration proposed below (see review Kashlinsky et al. 2018). The Y, J, H, K bands displayed approximate the bands available on *Euclid* and *Roman*.

Fig. 1b shows the expected CIB dipole assuming 1) the entire CMB dipole is of kinematic origin, and 2) no excess in CIB levels above that from known galaxies (Kashlinsky et al. 2018). If CMB traces the Universe’s rest-frame the CIB dipole should point in the CMB dipole direction and have the corresponding amplitude, eq. 1.

Fig. 1c compares the relative CB dipole at the near-IR bands with previous probes. At the near-IR bands the CB dipole should be amplified over that of the CMB to $(d_{\nu}/I_{\nu}) \simeq (3.1-5.5)D_{\text{CMB}} \simeq (4-7) \times 10^{-3}$. The higher amplification coupled with the wide sky coverage will result in the high precision CIB dipole measurement if foregrounds can be eliminated as discussed below.

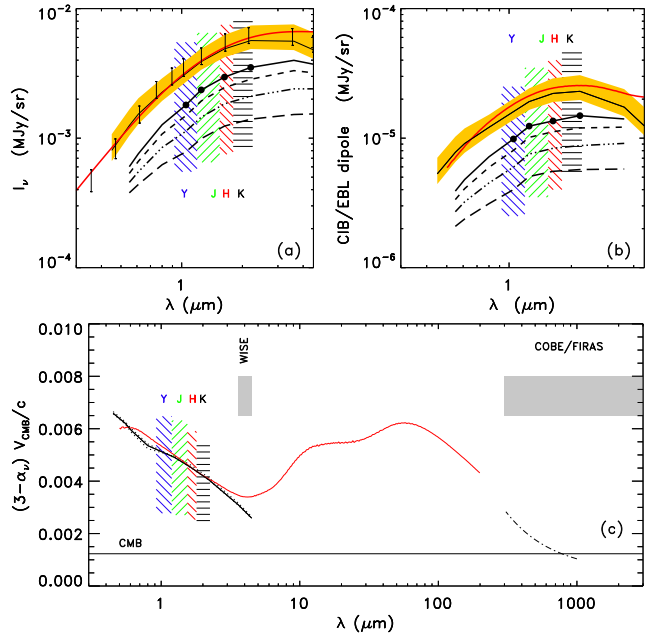


Figure 1. (a) CIB I_{ν} : black errors show CIB by the net observed deep counts, yellow is the HRK reconstruction (Helgason et al. 2012) with the solid black line showing the default model. Red line is from Driver et al. (2016). Black thick lines cover CIB from galaxies over $m_0 < m < m_1$ with $m_0 = 18, 19, 20, 21$ (solid, dashed, dashed-triple-dotted, long-dashed). Filled circles are for galaxies over $18 \leq m_{\text{AB}} \leq 24$. (b) CIB dipole if the entire CMB dipole is kinematic. The near-IR filters are marked. (c) CB dipole amplitude from optical to sub-mm shows the advantage of the near-IR configuration over previous studies employing sub-mm COBE/FIRAS low angular resolution data (Fixsen & Kashlinsky 2011) and mid-IR WISE AGN catalog (Secrest et al. 2021). Black lines are for the HRK-reconstructed CIB (dotted lines show the HFE→LFE spread), red line is the CIB/EBL from Driver et al. (2016), the black dashed-dotted line corresponds to the sub-mm CB amplification (Kashlinsky 2005); CMB dipole is marked.

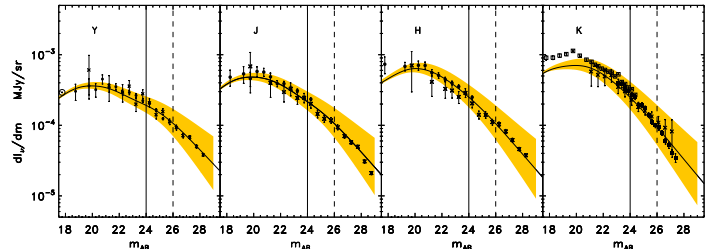


Figure 2. CIB from known galaxy populations. Data at Y, J, H are from (Windhorst et al. 2011, and refs therein) and at K from (Maihara et al. 2001; Keenan et al. 2010). Solid lines show the default HRK reconstruction and the shaded areas mark the HFE→LFE limits. Vertical solid and dashed lines mark *Euclid*’s Wide Survey’s and *Roman*’s magnitude limits. The measured K counts are taken as proxy for the *Roman* F184 band.

Fig. 2 shows the CIB build-up at the near-IR bands. The HRK-reconstructed CIB fits well the observed data; we use the reconstruction for estimates below, but when the data from the new forthcoming missions becomes available it will be used directly in the analysis.

The Solar System and Galaxy foregrounds present obstacles to probing the kinematic dipole nature using the *net* near-IR CIB. Based on examination of compiled zodiacal light observations (Leinert et al. 1998) and the DIRBE $100\mu\text{m}$ images (Hauser et al. 1998), we estimate uncorrected near-IR dipoles in Fig. 3 (top) for

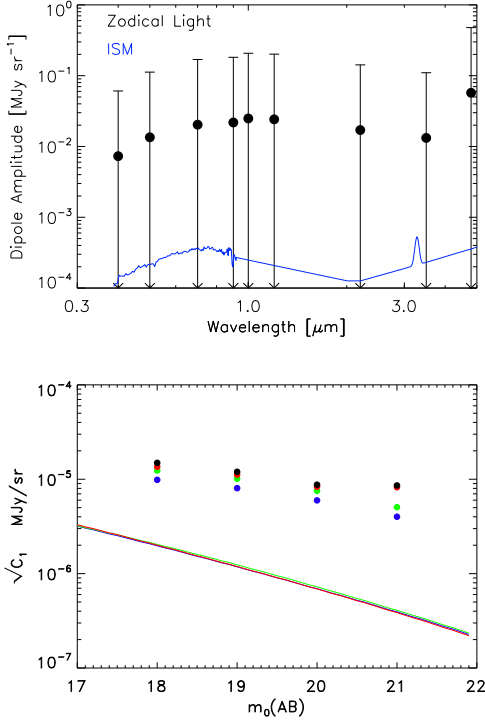


Figure 3. Top: Zodiacal light dipole in near-IR bands could be ~ 0.1 MJy sr^{-1} if measured at elongations $\sim 90^\circ \pm 10^\circ$ on a single day (black upper limits). When averaged over long periods (> 1 year), the net dipole amplitude should decrease by an order of magnitude (black dots). The dipole amplitude from scattered light and emission by the diffuse ISM (blue line) from scaling the measured $100 \mu\text{m}$ emission after masking 85% of the sky such that the measurements are from only the lowest brightness regions near the Galactic poles. Subtracting models of the zodiacal light and ISM/cirrus-scattered light may reduce these by over an order of magnitude. **Bottom:** The lines show the clustering dipole at $m_1 = 24$ vs m_0 with the color notation for the Y,J,H,K bands from Fig. 1. Blue, green, red, black circles show the dipole expected at the given m_0 for Y, J, H, K bands. In the K (F184) band *Roman* will go 2 magnitudes deeper which will help reduce further the clustering dipole.

observations constrained to solar elongations near 90° (as is common for space-based observations). The apparent dipole on a given date is $d_{\text{Zodi}} \sim 0.11$ MJy sr^{-1} at $1.25 \mu\text{m}$. Since the direction of this dipole varies annually, averaging over one or more years reduces its net amplitude by $\sim 10\times$. Even if the zodiacal light is modeled/subtracted with 1% accuracy, the residual dipole interferes with the CIB dipole. The cirrus dipole was estimated by simultaneous fitting for the monopole+dipole+quadrupole map components with several increasingly severe masks defined by brightness and Galactic and ecliptic latitude. The minimum dipole amplitude is ~ 0.1 MJy sr^{-1} at $100 \mu\text{m}$ (similar to Fixsen & Kashlinsky 2011). The dipole is oriented toward the Galactic center, even in the heavily masked cases. We scale the $100 \mu\text{m}$ ISM dipole amplitude to the shorter wavelengths using the ISM colors from Arendt et al. (1998); Sano et al. (2016). This yields a $1.25 \mu\text{m}$ ISM/cirrus dipole 2×10^{-4} MJy sr^{-1} , $\sim 10\times$ greater than the expected CIB dipole. To measure the CIB dipole would require subtracting the ISM model with sub-percent accuracy. However, measurements of ISM colors typically show variation by factors of a few at different sky locations. Thus, while a simple scaling of the far-IR ISM emission can be used to estimate the near-IR ISM dipole amplitude, it is unlikely to be sufficient here so *foregrounds*

present a substantial problem for probing the dipole of the net CIB. The problem can be resolved with the method proposed next.

2 IGL DIPOLE FROM SPACE-BORNE WIDE SURVEYS

To overcome the obstacles from foreground dipoles, we use the all-sky part of the CIB known as IGL (Integrated Galactic Light), reconstructed from resolved galaxies in a space-borne wide survey,

$$I_\nu(l, b) = S_0 \int_{m_0}^{m_1} 10^{-0.4m} \left[\frac{dN_\nu}{dm} \right] dm \quad (2)$$

where $S_0 = 3.631 \times 10^{-3}$ MJy, with m_0 suitably selected to remove the galaxy clustering dipole and m_1 imposed by the wide survey sensitivity limits. Here we will want to measure the dipole in the flux, not the number counts. For the dipole measurement the IGL will be constructed from the survey by adding fluxes from galaxies within the magnitude limit over each field-of-view (FOV) centered at (l, b) with $> 10^5$ galaxies/deg 2 at $20 < m_{\text{AB}} < 24$ (e.g. Windhorst et al. 2011; Driver et al. 2016); it has similar spectral dependence to the CIB in Fig.1. To measure CIB dipole at the near-IR bands with S/N significance requires $\approx (S/N) (I_\nu/d_\nu)^2$ sources achieving $(S/N) \gtrsim (10-25)$ with 10^6 independent positions if $d_\nu \sim (3-5) \times 10^{-3} I_\nu$ if foregrounds can be overcome. *Euclid* (Laureijs et al. 2011) will cover $\sim 15,000$ deg 2 in Y, J, H bands to $m_{\text{AB}} = 24$ beyond the peak of their CIB contribution and *Roman* (Spergel et al. 2015) is planned to cover $\sim 2,000$ deg 2 in Y, J, H and K (taken to approximate F184 by *Roman*, Akeson et al. (2019)) filters.

Foregrounds contribute negligibly to the IGL dipole, being removed locally in galaxy samples at an unprecedented precision (Scaramella et al. 2021). Additionally, zodi is known to have no spatial fluctuations to very low levels (e.g. Arendt et al. 2016) and Galactic cirrus has negligible fluctuation power (Gautier et al. 1992) on individual galaxy scales (see further refs in Kashlinsky et al. 2018).

The CIB dipole from galaxy clustering decreases with fainter galaxies (Gibelyou & Huterer 2012) and/or sources at higher z , constraining m_0 . As part of their dark energy science, *Euclid* will measure spectroscopic redshifts over its extragalactic sky out to $z=2.1$ while *Roman* will go deeper. The source redshift distribution is expected to have a mean at $z \sim 0.9$ with a density of 30 galaxies per square arcmin (Laureijs et al. 2011) and luminous giant galaxies can be detected out to $z \sim 3$; the linear scales subtended by the dipole at these epochs are well into the Harrison-Zeldovich regime. Fig.3 bottom shows the remaining clustering dipole for galaxies with $m_0 < m < m_1$ compared with the CIB dipole if the CMB dipole is kinematic. It was computed from the HRK reconstruction of CIB power with $m_1 = 24$ for Y/J/H/K which follows the Harrison-Zeldovich regime at large angular scales, i.e. $P = A(m_0)\ell$. We then evaluate, with HRK reconstruction, $A(m_0)$ for given m_0 with the above m_1 , and take the CIB dipole from clustering as $d_\nu = \sqrt{C_1}$ with the rms dipole $C_1 = A(m_0)/\pi$. Additionally, cosmic variance affects the measured dipole, so at 95 (99) per cent confidence level $d_\nu < 4(5.7)\sqrt{C_1}$. Selecting $m_0 \sim (18-21)$ leaves $\sqrt{C_1}$ over an order of magnitude below that expected from the kinematic CMB dipole.

That configuration, eq.2, has additional contribution to the dipole due the local motion $\Delta m = -(2.5 \lg e) [1 + \eta(m)] \frac{V}{c} \cos \Theta$ for CIB sources with SED $f_\nu \propto \nu^\eta$ (Ellis & Baldwin 1984; Itoh et al. 2010). In that case the dipole eq. 1 will be modified by the $m_{0,1}$ variation:

$$d_\nu(m_0 < m < m_1) = [(3 - \alpha_{\nu, m_0 < m < m_1}) + \Delta\alpha_\nu] \frac{V}{c} \bar{I}_\nu(m_0 < m < m_1)$$

Table 1. HRK-reconstructed $N_{\text{tot}}(m_0 < m < m_1)/10^6$ per 1,000 deg²

Filter	Y	J	H	K
m_0	$m_1=24/26$	$m_1=24/26$	$m_1=24/26$	$m_1=26$
18	85.6/347.0	105.2/375.8	128.8/411.3	422.7
19	84.9/346.2	104.3/372.2	127.7/410.1	421.2
20	82.9/344.2	101.6/372.7	124.2/406.6	417.0
21	78.0/339.4	95.2/365.7	115.8/398.3	407.2

(3)

with

$$\Delta\alpha_\nu = \frac{\frac{dI_\nu}{dm}|_{m_1}}{\bar{I}_\nu(m_0 < m < m_1)} [1 + \eta(m_1)] - \frac{\frac{dI_\nu}{dm}|_{m_0}}{\bar{I}_\nu(m_0 < m < m_1)} [1 + \eta(m_0)] \quad (4)$$

Figs. 1, 2 show that at the values $m_{0,1}$ selected here over the near-IR bands the galaxy CIB contribution is only $\frac{dI_\nu}{dm}|_{m_{0,1}} \sim$ (a few percent) $\bar{I}_\nu(m_0 < m < m_1)$. At these wavelengths one would probe galaxy stellar populations at various parts of the restframe spectrum, which is theoretically well studied and with effective $\eta \sim -2$, depending on the age, mass-function, metallicity and epoch of the populations leading to $\Delta\alpha_\nu \ll \alpha_\nu$. When the measurement is performed, the values of η and their distribution will be measurable for the cataloged galaxies and $\alpha, \Delta\alpha$ will be reconstructed directly. Fig. 1 shows that the considered here CIB has a robust value of α at the near-IR wavelengths making the application of the CIB-based eq. 3 advantageous to achieving robust results with a high statistical accuracy. The statistical signal/noise for the dipole at each band is:

$$\left(\frac{S}{N}\right)_\nu = 127 \frac{(3 - \alpha_{\nu, m_0 < m < m_1}) D_{\text{CMB}}}{4 \times 10^{-3}} \sqrt{\frac{N_{\text{tot}}}{10^9}} \quad (5)$$

Overall such S/N can achieve sub-degree direction resolution.

Table 1 shows the HRK-reconstructed number of galaxies, N_{tot} , expected in *Euclid* data with $m_0 < m < m_1$ at $m_1 = 24$ and the *Roman* mission at $m_1 = 26$ over a smaller area, but extending to K band shown in the last column. When CMB dipole is entirely kinematic the CIB/IGL dipole components would be $S_i = (d_\nu/I_\nu)n_i$ in the direction $\hat{n} = (-0.07, -0.66, 0.75)$. Its direction uncertainties were evaluated per Atrio-Barandela et al. (2010): the error on S_i is given by that on the mean, $N_{\text{tot}}^{-1/2}$, weighted by the dispersion of the direction cosines on the sky area $4\pi f_{\text{sky}}$ covered by the survey, i.e., $N_i = 1/(N_{\text{tot}}\langle n_i^2 \rangle)^{1/2}$ with $\langle n_i^2 \rangle = (4\pi)^{-1} \int_{4\pi f_{\text{sky}}} n_i^2 d\Omega$. We adopt the configurations from Table 1. Fig. 4 shows the resultant S/N accumulation for the CIB dipole components in each band for the two missions. (For the *Euclid* example we used the projected sky coverage from Laureijs et al. (2020). For *Roman* the area that will be observed has not been yet finalized. For our estimates we used an area of $\sim 1,700$ deg² bounded in R.A. and Dec by $10 \leq \alpha < 60$ and $-50 \leq \delta < -10$. We call this area the Southern *Roman* patch. Since the satellite could be observing a larger area, we also considered the final area to include another symmetric Northern *Roman* patch, limited by $190 \leq \alpha < 240$ and $10 \leq \delta < 50$.) The Z-component's S/N is the largest because of the planned avoidance of Galactic and Ecliptic planes.

Generally, the CIB/IGL dipole direction will be well determined in these configurations with errors decreasing $\propto N_{\text{tot}}^{-1/2}$ for the configurations in Table 1. If the CIB dipole points in the CMB dipole's

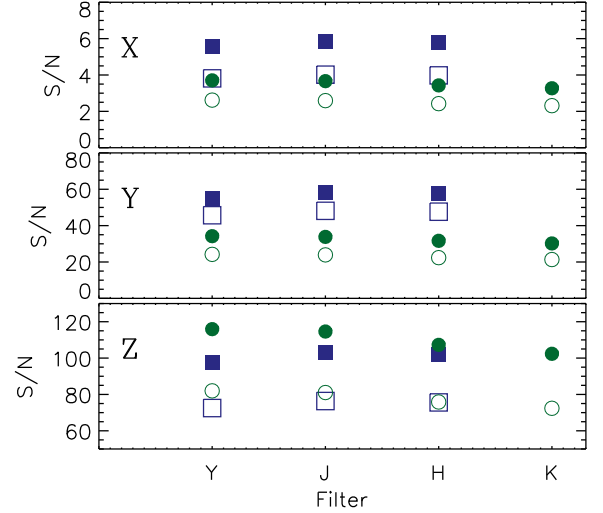


Figure 4. S/N for each of the *Euclid* (squares) and *Roman* (circles) photometric bands. Open symbols show 3 yrs of *Euclid* and the Southern patch of *Roman*. Filled symbols correspond to 6 yrs of *Euclid* and the Southern+Northern *Roman* patches. Other configurations would have $S/N \propto N_{\text{tot}}^{1/2}$.

direction, the directional uncertainty would be:

$$\Delta\Theta(90\%, 95\%, 99\%) = (1.8^\circ, 2^\circ, 2.6^\circ) \left(\frac{N_{\text{tot}}}{10^9}\right)^{-1/2} \quad (6)$$

3 DISCUSSION

The IGL can measure the CIB dipole with $S/N \gtrsim 50-100$, testing the kinematic origin of the CMB dipole to $\sim 1^\circ$. Eq 2 can be subdivided into narrow magnitude bins ($m_0 \rightarrow m_1$) where η does not vary significantly but can be evaluated with the available data. Since the CIB dipole due to local motion should be independent of redshift, probing it for sources within various redshift ranges to $z \approx 3$ will help establish its kinematic origin. If the primordial component turns out to be present, it could be generated by isocurvature perturbations of pre-inflationary origin, opening a window to probe the superhorizon structure of the Universe prior to inflation.

By construction, there would not be any zodi or ISM impacts on the IGL dipole. Any IGL dipole should fall with λ in accordance with Fig. 1 while the foregrounds at the near-IR wavelengths come from reflected light (Kelsall et al. 1998; Arendt et al. 1998) and rise steeply toward the visible, providing a consistency test. If there is a systematic in the photometric zeropoints that has a dipole component, this will give a false dipole signature. Given the expected CIB dipole of $\approx 0.5\%$, one needs these systematics at $\lesssim 0.1\%$.

Extinction corrections (ECs) are important in the application of this method as discussed by Secrest et al. (2021) who found the effect small. They are more important in visible than in the near-IR bands and the *Roman*'s K band is where extinction is smallest. Scaling the E(B-V) reddening maps of Schlegel et al. (1998) indicates that without ECs the dipole amplitude may be comparable with the IGL dipole. A direct approach to reduce this contribution is to apply an extinction correction to the photometry of the individual galaxies before calculating the IGL (Secrest et al. 2021). ECs must be sufficiently accurate so any residual errors are small compared to the expected signal. Models can fit reddening coefficients or colors to a

few percent (e.g. Scaramella et al. 2021). The analyses could be restricted to low extinction areas. The cosmic dipole can be determined with an error $\lesssim 10^\circ$ (90% c.l.) with some 10^8 galaxies and the error is even smaller for other configurations in Table 1. Then, the analysis can be extended to larger areas. All the measured dipoles, further probed by *Roman* at greater depths, should be consistent and point in the same direction within the errors with the amplitude scaling as in Fig. 1 for all the selected patches, bands and configurations.

Galactic stars-galaxies separation is necessary to avoid a spurious dipole from stars, which can dominate source counts at $m \lesssim 18\text{--}20$ in high latitude fields (e.g. Windhorst et al. 2011; Ashby et al. 2013). Simple solutions based on source size (e.g. Windhorst et al. 2011) will suffice here, because the exclusion of all compact sources will eliminate a Galactic stellar dipole, and it will not induce a cosmic dipole if compact extragalactic sources are inadvertently excluded. The further advantage of the forthcoming space missions' sub-arcsec angular resolution is the ability to resolve the galaxies individually, robustly overcoming source-confusion.

This bodes well for a high precision measurement of the CIB dipole necessary to resolve the kinematic nature of the CMB dipole. The primordial CMB dipole component will be estimated robustly from the measured IGL dipole using Fig. 1 to transform to velocity then converted into the kinematic CMB component to be subtracted from the CMB dipole of highly precise amplitude and direction.

ACKNOWLEDGEMENTS

We particularly thank Rick Arendt for contributions to understanding the role of foregrounds and other systematics and Kari Helgason for the HRK reconstruction used here. FAB acknowledges Grants PGC2018-096038-B-I00 (MINECO and FEDER, "A way of making Europe") and SA083P17 from the Junta de Castilla y León.

DATA AVAILABILITY

No proprietary data were used here. The public data presented will be shared on reasonable request to the lead author (AK).

REFERENCES

Akeson R., et al., 2019, arXiv e-prints, [p. arXiv:1902.05569](https://arxiv.org/abs/1902.05569)
 Arendt R. G., et al., 1998, *ApJ*, **508**, 74
 Arendt R. G., Kashlinsky A., Moseley S. H., Mather J., 2016, *ApJ*, **824**, 26
 Ashby M. L. N., et al., 2013, *ApJ*, **769**, 80
 Atrio-Barandela F., 2013, *A&A*, **557**, A116
 Atrio-Barandela F., Kashlinsky A., Ebeling H., Kocevski D., Edge A., 2010, *ApJ*, **719**, 77
 Atrio-Barandela F., Kashlinsky A., Ebeling H., Fixsen D. J., Kocevski D., 2015, *ApJ*, **810**, 143
 Colin J., Mohayaee R., Rameez M., Sarkar S., 2019, *A&A*, **631**, L13
 Das K. K., Sankharva K., Jain P., 2021, *J. Cosmology Astropart. Phys.*, **2021**, 035
 Driver S. P., et al., 2016, *ApJ*, **827**, 108
 Ellis G. F. R., Baldwin J. E., 1984, *MNRAS*, **206**, 377
 Erdoğan P., et al., 2006, *MNRAS*, **373**, 45
 Fabian A. C., Warwick R. S., 1979, *Nature*, **280**, 39
 Fixsen D. J., Kashlinsky A., 2011, *ApJ*, **734**, 61
 Fixsen D. J., et al., 1994, *ApJ*, **420**, 445
 Gautier T. N. I., Boulanger F., Perault M., Puget J. L., 1992, *AJ*, **103**, 1313
 Gibelyou C., Huterer D., 2012, *MNRAS*, **427**, 1994
 Gleeson L. J., Axford W. I., 1968, *Ap&SS*, **2**, 431
 Grishchuk L. P., 1992, *Phys. Rev. D*, **45**, 4717

Gunn J. E., 1988, in van den Bergh S., Pritchet C. J., eds, *Astronomical Society of the Pacific Conference Series Vol. 4, The Extragalactic Distance Scale*. p. 344
 Hauser M. G., et al., 1998, *ApJ*, **508**, 25
 Helgason K., Ricotti M., Kashlinsky A., 2012, *ApJ*, **752**, 113
 Itoh Y., Yahata K., Takada M., 2010, *Phys. Rev. D*, **82**, 043530
 Jain P., Ralston J. P., 1999, *Modern Physics Letters A*, **14**, 417
 Kashlinsky A., 2005, *Phys. Rep.*, **409**, 361
 Kashlinsky A., Tkachev I. I., Frieman J., 1994, *Phys. Rev. Lett.*, **73**, 1582
 Kashlinsky A., Arendt R. G., Mather J., Moseley S. H., 2005, *Nature*, **438**, 45
 Kashlinsky A., Arendt R. G., Mather J., Moseley S. H., 2007a, *ApJ*, **654**, L1
 Kashlinsky A., Arendt R. G., Mather J., Moseley S. H., 2007b, *ApJ*, **654**, L5
 Kashlinsky A., Atrio-Barandela F., Kocevski D., Ebeling H., 2008, *ApJ*, **686**, L49
 Kashlinsky A., Atrio-Barandela F., Kocevski D., Ebeling H., 2009, *ApJ*, **691**, 1479
 Kashlinsky A., Atrio-Barandela F., Ebeling H., Edge A., Kocevski D., 2010, *ApJ*, **712**, L81
 Kashlinsky A., Atrio-Barandela F., Ebeling H., 2012a, arXiv e-prints, [p. arXiv:1202.0717](https://arxiv.org/abs/1202.0717)
 Kashlinsky A., Arendt R. G., Ashby M. L. N., Fazio G. G., Mather J., Moseley S. H., 2012b, *ApJ*, **753**, 63
 Kashlinsky A., Arendt R. G., Atrio-Barandela F., Cappelluti N., Ferrara A., Hasinger G., 2018, *Reviews of Modern Physics*, **90**, 025006
 Kashlinsky A., et al., 2019, *BAAS*, **51**, 37
 Keenan R. C., Trouille L., Barger A. J., Cowie L. L., Wang W. H., 2010, *ApJS*, **186**, 94
 Kelsall T., et al., 1998, *ApJ*, **508**, 44
 King A. R., Ellis G. F. R., 1973, *Communications in Mathematical Physics*, **31**, 209
 Kocevski D. D., Ebeling H., 2006, *ApJ*, **645**, 1043
 Kogut A., et al., 1993, *ApJ*, **419**, 1
 LIBRAE 2013, Looking at Infrared Background Radiation Anisotropies with *Euclid*, <https://www.euclid.caltech.edu/page/KashlinskyTeam>
 Lauer T. R., Postman M., 1992, *ApJ*, **400**, L47
 Laureijs R., et al., 2011, arXiv e-prints, [p. arXiv:1110.3193](https://arxiv.org/abs/1110.3193)
 Laureijs R., et al., 2020, in *Society of Photo-Optical Instrumentation Engineers (SPIE) Conference Series*. p. 114430F, [doi:10.1117/12.2563145](https://doi.org/10.1117/12.2563145)
 Lavaux G., Tully R. B., Mohayaee R., Colombi S., 2010, *ApJ*, **709**, 483
 Leinert C., et al., 1998, *A&AS*, **127**, 1
 Ma Y.-Z., Gordon C., Feldman H. A., 2011, *Phys. Rev. D*, **83**, 103002
 Maihara T., et al., 2001, *PASJ*, **53**, 25
 Mathewson D. S., Ford V. L., Buchhorn M., 1992, *ApJ*, **389**, L5
 Matzner R. A., 1980, *ApJ*, **241**, 851
 Mersini-Houghton L., Holman R., 2009, *J. Cosmology Astropart. Phys.*, **2009**, 006
 Migkas K., Schellenberger G., Reiprich T. H., Pacaud F., Ramos-Ceja M. E., Lovisari L., 2020, *A&A*, **636**, A15
 Nodland B., Ralston J. P., 1997, *Phys. Rev. Lett.*, **78**, 3043
 Peebles P. J., Wilkinson D. T., 1968, *Physical Review*, **174**, 2168
 Sano K., Matsuura S., Tsumura K., Arai T., Shirahata M., Onishi Y., 2016, *ApJ*, **821**, L11
 Scaramella R., et al., 2021, arXiv e-prints, [p. arXiv:2108.01201](https://arxiv.org/abs/2108.01201)
 Schlegel D. J., Finkbeiner D. P., Davis M., 1998, *ApJ*, **500**, 525
 Secrest N. J., von Hausegger S., Rameez M., Mohayaee R., Sarkar S., Colin J., 2021, *ApJ*, **908**, L51
 Singal A. K., 2011, *ApJ*, **742**, L23
 Spergel D., et al., 2015, arXiv e-prints, [p. arXiv:1503.03757](https://arxiv.org/abs/1503.03757)
 Tiwari P., Kothari R., Jain P., 2022, *ApJ*, **924**, L36
 Turner M. S., 1991, *Phys. Rev. D*, **44**, 3737
 Villumsen J. V., Strauss M. A., 1987, *ApJ*, **322**, 37
 Wiltshire D. L., Smale P. R., Mattsson T., Watkins R., 2013, *Phys. Rev. D*, **88**, 083529
 Windhorst R. A., et al., 2011, *ApJS*, **193**, 27